Atmos. Meas. Tech. Discuss., https://doi.org/10.5194/amt-2018-20
Manuscript under review for journal Atmos. Meas. Tech.
Discussion started: 31 January 2018

Atmospheric Measurement Techniques Discussions

Reducing representativeness and sampling errors in radio occultation–radiosonde comparisons

Shay Gilpin [1], Therese Rieckh [1,2], and Richard Anthes [1]

[1]COSMIC Program Office, University Corporation for Atmospheric Research, Boulder, CO
[2]Wegener Center for Climate and Global Change, University of Graz, Austria

Correspondence to: Shay Gilpin (sgilpin@ucar.edu)

Abstract. Radio occultation (RO) and radiosonde (RS) comparisons provide a means of analyzing errors associated with both observational systems. Since RO and RS observations are not taken at the exact same time or location, temporal and spatial sampling errors resulting from atmospheric variability can be significant and inhibit error analysis of the observational systems. In addition, the vertical resolutions of RO and RS profiles vary and vertical representativeness errors may also affect the comparison. Typically in RO–RS comparisons, RS observations are co-located with RO profiles within a fixed time window and distance, i.e. within 3 – 6 h and circles of radii ranging between 100 – 500 km. In this study, we first show that vertical filtering of RO and RS profiles to a common vertical resolution reduces representativeness errors. We then test two methods of reducing horizontal sampling errors during RO–RS comparisons: restricting co-location pairs to within ellipses oriented along the direction of wind flow rather than circles, and applying a spatial correction based on model data. We compare RO and RS differences at four GCOS Reference Upper-Air Network (GRUAN) RS stations in different climatic locations in which co-location pairs were constrained to a large circle (∼666 km radius), small circle (∼300 km radius) and ellipse parallel to the wind direction (∼666 km semi-major axis, ∼133 km semi-minor axis). We also apply a spatial correction using European Centre for Medium-Range Weather Forecasts Interim Reanalysis (ERA-Interim) gridded data. Restricting co-locations to within the ellipse reduces root mean square (RMS) refractivity, temperature, and water vapor pressure differences relative to RMS differences within the large circle, and either reduce or are comparable to RMS differences within circles of similar area. Applying the spatial correction shows the most significant reduction in RMS differences, such that RMS differences are nearly identical with the spatial correction regardless of the geometric constraints. We conclude that implementing the spatial correction using a reliable model will most effectively reduce sampling errors during RO–RS comparisons, however if a reliable model is not available, restricting spatial comparisons to within an ellipse parallel to the wind flow will reduce sampling errors caused by horizontal atmospheric variability.

1 Introduction

Radio occultation (RO), a relatively new method of atmospheric measurements, has established itself as an important atmospheric observational system. By measuring the phase delay of radio-waves sent from Global Positioning Satellites (GPS) traversing horizontally through Earth's atmosphere to low-Earth orbiting satellites, RO obtains accurate and precise vertical

Atmos. Meas. Tech. Discuss., https://doi.org/10.5194/amt-2018-20
Manuscript under review for journal Atmos. Meas. Tech.
Discussion started: 31 January 2018

Atmospheric Measurement Techniques Discussions

profiles of bending angles. Refractivity is obtained from inverting bending angle profiles using the Abel Transform, and from refractivity, stratospheric temperature and tropospheric temperature and water vapor can be retrieved (where tropospheric temperature and water vapor require auxiliary measurements or model data). RO provides observations with global coverage, high vertical resolution, little or no instrument bias, and bending angles which can be directly assimilated into numerical weather prediction models (Melbourne et al., 1994; Kursinski et al., 1997; Anthes et al., 2008).

Since the proof-of-concept GPS/MET mission in 1995 (Ware et al., 1996), RO profiles of refractivity, temperature, and water vapor have been compared to radiosondes (RS) to assess the quality of RO retrievals and the performance of RS instruments. RS are considered a standard for comparison due their long history of in situ measurements starting in 1958 (Ho et al., 2017), and several studies have used RS as a reference for RO retrieval analysis (Wickert et al., 2004; Kuo et al., 2005; He et al., 2009; Xu et al., 2009; Ho et al., 2010; Sun et al., 2010; Zhang et al., 2011; Wang et al., 2013; Vergados et al., 2014). Conversely, due to RO's properties of high accuracy and precision, high vertical resolution, and global coverage, RO has been used to evaluate the performance of various RS instruments. For example, Kuo et al. (2005) demonstrated that RO observations are of high enough resolution to differentiate between RS instruments and asses their performance, particularly instrument biases due to geographic region, radiation errors, day/night biases, etc.

One of the main difficulties associated with RO–RS comparisons comes from temporal and spatial differences between nearby RS and RO soundings. Since both measurements are not taken at the exact same time or location, temporal and spatial errors (sampling errors) can be a significant part of the computed RO–RS differences. To reduce the effects of sampling errors, the majority of previous studies have restricted co-located RO observations within a fixed time range and distance, typically within $3-6\,\mathrm{h}$ of the RS launch and within circles of radii ranging from $100-500\,\mathrm{km}$ centered at the RS launch site. Alternatively, Staten and Reichler (2009) used smaller radii circles ($3-36\,\mathrm{km}$) and fitted a second order polynomial to the root mean square (RMS) differences in order to filter out atmospheric variability. Weather-scale atmospheric variability within these circles and time ranges is the major cause of these sampling errors (Sun et al., 2010), and in this study we attempt to reduce these errors.

We apply two methods to reduce sampling errors caused by atmospheric variability in RO–RS comparisons. First, we restrict co-location pairs to within ellipses oriented along the direction of wind flow rather than circles. Orienting ellipses along the direction of wind flow should minimize atmospheric variability due to the interdependence of atmospheric composition and wind. Temperature and water vapor gradients in the free atmosphere tend to be perpendicular to wind flow, resulting in refractivity (a function of both temperature and water vapor pressure) gradients to also approximately lie perpendicular to wind flow. Therefore, we hypothesize that the spatial variability of refractivity within ellipses of semi-major axis a oriented along the wind direction will be reduced compared to the variability within circles of radius a. The second method consists of applying a spatial correction to the RO–RS co-location pairs based on European Centre for Medium-Range Weather Forecasts Interim Reanalysis (ERA-Interim) model data (see www.ecmwf.int/era). By subtracting the model data from both the RO and RS the background and representativeness errors are removed, leaving only the RO and RS observational errors. The approach has been called the "double-difference" method (Haimberger et al., 2012; Wong et al., 2015; Tradowsky et al., 2017). In addition

Atmos. Meas. Tech. Discuss., https://doi.org/10.5194/amt-2018-20
Manuscript under review for journal Atmos. Meas. Tech.
Discussion started: 31 January 2018

Atmospheric Measurement Techniques Discussions

to the sampling error, the different vertical resolution of the RO and RS profiles can lend to representativeness errors when compared. To reduce these errors, we filter the profiles to a common vertical resolution before the comparisons.

Although this paper considers RO–RS comparisons, the filtering and methods of reducing sampling errors can be applied to comparisons of other data pairs, such as any two sounding systems or observations and models. However, the amount of filtering and the geometric constraints on the co-location pairs may have to be adjusted for different comparisons. For example, comparisons of RO or RS soundings with infrared (IR) or microwave (MW) soundings, which have much different vertical resolutions, would require a greater filtering of the RO or RS profiles to make them comparable to the lower-resolution profiles.

The first section describes the data sets, filtering methods, and methodology implemented in this study. Next, we discuss aspects of the ellipse co-location method conducted using the Lindenberg RS station. The following section describes the results of co-locations using both the ellipse and spatial correction methods at four different RS stations. In the final section we summarize the results and discuss further impacts and implications.

2 Methods

2.1 RO and RS data sets

All RO profiles are provided by the COSMIC Data Analysis and Archive Center (CDAAC), which can be found at http://cdaac-www.cosmic.ucar.edu. RO refractivity, temperature, and water vapor pressure profiles are taken from the wetPrf profiles provided on a uniform 100 m mean sea level height grid. All available processed, high-quality profiles from the COSMIC-1, GRACE 1 and 2, and Metop-A/B missions during the time periods of comparisons are used.

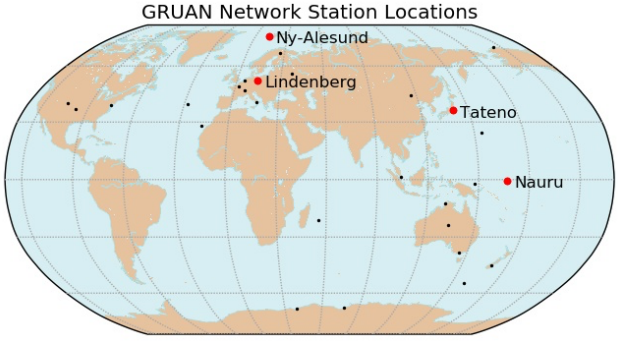

Figure 1. Map of GRUAN RS network. Labeled locations with red dots are RS stations used in this study, black dots mark the other GRUAN network RS stations.

All RS profiles are provided by the Global Climate Observing System (GCOS) Reference Upper-Air Network (GRUAN) and downloaded from National Oceanic and Atmospheric Administration (NOAA) National Climatic Data Center. We chose four stations in different climates for this study: Lindenberg, Germany (LIN); Ny-Ålesund, Norway (NYA); Tateno, Japan (TAT); and Nauru, Nauru (NAU) for the following time periods: 2014, 2013, 2012, and 2011-2013, respectfully. (Nauru is the

Atmos. Meas. Tech. Discuss., https://doi.org/10.5194/amt-2018-20
Manuscript under review for journal Atmos. Meas. Tech.
Discussion started: 31 January 2018

Atmospheric Measurement Techniques Discussions

only station in which the full period of activation was used; this is due to the low number of RS launches during 2011 through late August 2013.) Figure 1 is a map of the GRUAN RS stations with the locations of the four stations used in this study labeled and marked in red. All four stations use the Vaisala RS92 radiosonde instruments (for details on GRUAN RS processing see Dirksen et al., 2014). For refractivity comparisons, RS refractivity is computed under the assumption of a neutral atmosphere (Smith and Weintraub, 1953):

$$N = 77.6\frac{P}{T} + 3.73 \times 10^5 \frac{e}{T^2} \tag{1}$$

where N is refractivity ($\mathrm{N-units}$), P is dry air pressure (hPa), T is temperature (Kelvin) and e is water vapor pressure (hPa).

We generate two data sets: an unfiltered data set which contains all original RO and RS profiles, and a filtered data set containing the vertically filtered versions of the original RO and RS profiles.

2.2 Filtering

Representativeness errors result from two different aspects of the RO and RS observations: (1) GRUAN RS have a temporal resolution of 1 s, with vertical resolution of 5 – 10 m on average (Ladstädter et al., 2015), which is much finer than the 100 m vertical resolution of the RO wetPrf profiles, and (2) RS observations are a series of point measurements, whereas RO observations are weighted averages of a cylindrical volume of atmosphere with horizontal scales of 150 – 300 km (Kursinski et al., 1997; Kuo et al., 2004; Anthes, 2011). Vertical filtering of both RO and RS profiles should decrease the representativeness errors caused by differences in vertical resolutions and observation types, resulting in a more meaningful comparison between profiles. Removal of structures with very small vertical scales also has the effect of reducing representativeness errors associated with different horizontal scales (footprints) of the observations. Structures with very small vertical scales in the RS profile are likely associated with horizontal scales too small to be resolved by the RO observations. Though the majority of previous RO–RS comparison studies do not filter the RO or RS profiles before comparison, Kuo et al. (2004) filtered the profiles to remove structures with vertical scales less than 1 km before comparison with model analyses in an effort to minimize vertical sampling differences.

To remove small-scale, unrepresentative structures in both the RO and RS profiles, we applied the Savitzky-Golay low-pass filter (Savitzky and Golay, 1964). We first linearly interpolated profile variables (refractivity, temperature, and water vapor pressure) to a 10 hPa (∼100 m) uniform vertical grid, then filtered using a 40 hPa (∼400 m) filter window. We tested various combinations of filter windows and number of passes to determine the effects of filtering on the RS and RO profiles (not shown). The number of passes of the same filter result in minor smoothing effects relative to different filter windows, and filter windows larger than 40 hPa cause too much smoothing of the RS profile. RO profiles, due to their lower resolution relative to the RS profiles, demonstrated little change under different filter windows, therefore 40 hPa was chosen as a sufficient window to remove small scale features in the RS profile while preserving the overall structures of both the RS and RO profiles. To accommodate for the differences in vertical resolution, RO profiles underwent a single pass of the 40 hPa filter and RS profiles underwent three passes of the 40 hPa filter.

Atmos. Meas. Tech. Discuss., https://doi.org/10.5194/amt-2018-20
Manuscript under review for journal Atmos. Meas. Tech.
Discussion started: 31 January 2018

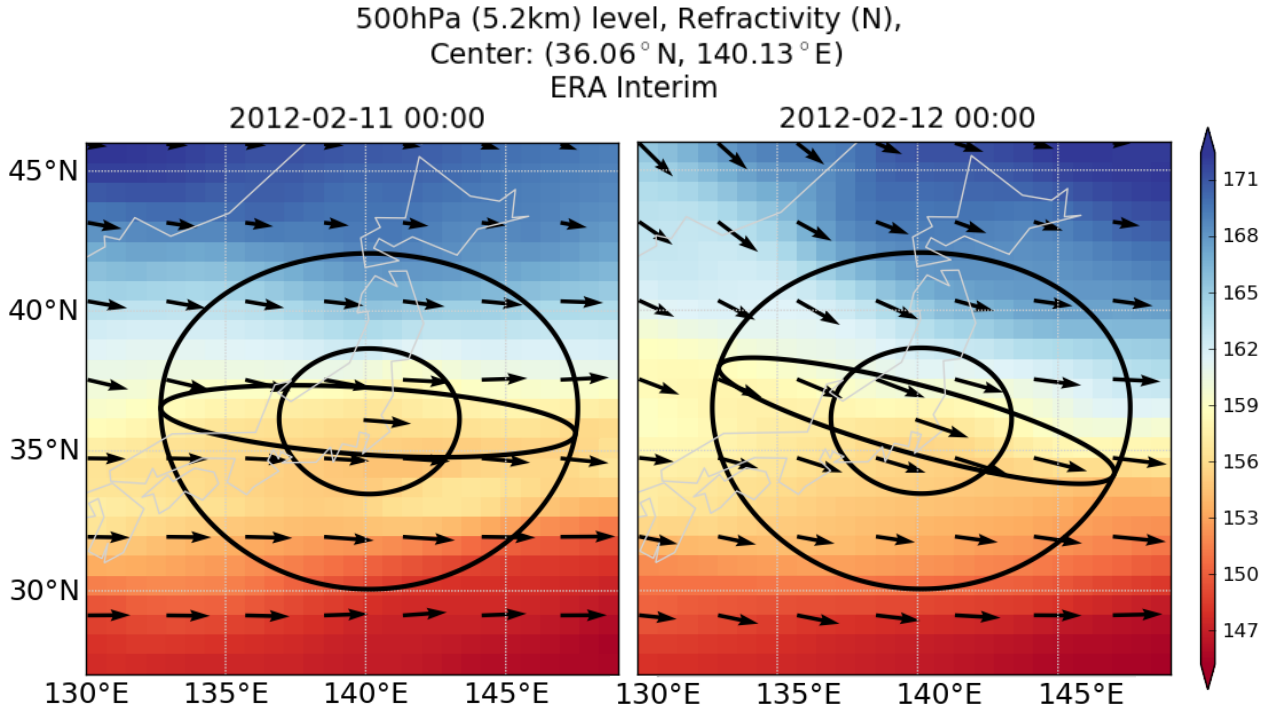

Figure 2. 500 hPa ERA-Interim refractivity field (color contours) at Tateno for Feb. 11 and 12, 2012 at 00:00 UTC. The three spatial geometries (large circle, small circle, ellipse) are shown in black centered at Tateno with wind vectors (black) denoting wind direction and magnitude. Generally, refractivity isopleths lie parallel to the wind flow, even as wind direction changes, resulting in minimal refractivity variability within the ellipse relative to both circles.

2.3 RO–RS co-location criteria and statistics

We co-located RO and RS observations using the ellipse method every 10 hPa between 1000 – 10 hPa at each RS location. We included RO occultations taken within 3 h of the RS launch at Ny-Ålesund, Tateno, and Nauru and within 1 h at Lindenberg due to the high number of RS launches (at least four times daily). We considered three different geometric constraints to co-locate RO profiles: (1) large circle of radius 6 ° latitude (∼666 km), (2) small circle of radius 2.6 ° latitude (∼300 km), and (3) ellipse parallel to the wind direction, 6 ° latitude semi-major axis and 1.2 ° latitude (∼133 km) semi-minor axis, each centered at the RS location. (The ellipse and small circle are circumscribed by the large circle, and the small circle was chosen such that the area within the small circle and ellipse are approximately the same, see Fig. 2). The X and Y coordinates of the points on the circles and ellipses are constructed using the following parameterization (a: semi-major axis, b: semi-minor axis, for circles

Atmos. Meas. Tech. Discuss., https://doi.org/10.5194/amt-2018-20
Manuscript under review for journal Atmos. Meas. Tech.
Discussion started: 31 January 2018

$a = b =$ radius, and both a, b are in km):

$$X(s) = a\cos(s)\cos(\theta) - b\sin(s)\sin(\theta)$$
$$Y(s) = a\cos(s)\sin(\theta) + b\sin(s)\cos(\theta) \quad (2)$$

where s is a parameter that varies between 0 and 2π and is stepped in increments of 0.01, yielding a series of 629 points that approximate the circle or ellipse, and θ is the wind direction in radians (converted from meteorological to polar coordinates). The X and Y coordinates of the circle or ellipse are first computed at the Equator where 1 ° of latitude and longitude equals 111 km, and then the X and Y coordinates are adjusted to the latitude and longitude of the RS station according to the following:

$$\mathrm{LAT}(Y,s) = \frac{Y(s)}{111} + \mathrm{LAT(RS)}$$
$$\mathrm{LON}(X,s) = \frac{X(s)}{111\cos(\mathrm{LAT}(Y,s))} + \mathrm{LON(RS)} \quad (3)$$

The ellipses change orientation such that the semi-major axis is parallel to the wind direction at each pressure level and time per RS. The circles remain fixed and unaffected by the change in wind direction, pressure level, or time.

Figure 2 illustrates the three geometries centered at Tateno at 500 hPa for two days in February, noting that the ellipse adjusts its orientation as wind direction changes with time and at a pressure level. Preliminary testing of the ellipse co-location method with ERA-Interim model refractivity fields confirmed that refractivity isopleths tend to follow wind flow (as illustrated in Fig. 2); thus orientation of the ellipse along the direction of the wind flow should increase atmospheric homogeneity relative to the large circle.

We computed differences for each co-location pair:

$$X_{\mathrm{RO–RS}} = X_{\mathrm{RO}} - X_{\mathrm{RS}} \quad (4)$$

where X refers to time, refractivity, temperature, and water vapor pressure. We computed the RMS of the differences for each pressure level over the full time period and used the RMS to quantify the reduction in sampling errors. In certain cases we also computed the percent difference between two quantities X_i and X_j:

$$\%\, diff = 100 * \frac{X_i - X_j}{X_j} \quad (5)$$

2.4 Spatial correction algorithm

Applying a spatial correction to the differences during RO–RS co-locations is an alternate method of reducing sampling errors in the presence of an auxiliary data set. This method has been applied in previous studies and is not restricted to RO–RS comparisons. Haimberger et al. (2012) used this approach to homogenize RS records. Wong et al. (2015) used ECMWF forecasts to estimate the sampling differences between Atmospheric Infrared Sounder (AIRS) and RS co-located pairs, using a double-difference error estimate to correct AIRS and RS differences. Tradowsky et al. (2017) calculated an observed – background (O – B) double-difference to estimate the mean RS temperature bias using co-located RO profiles and the Met

Atmos. Meas. Tech. Discuss., https://doi.org/10.5194/amt-2018-20
Manuscript under review for journal Atmos. Meas. Tech.
Discussion started: 31 January 2018

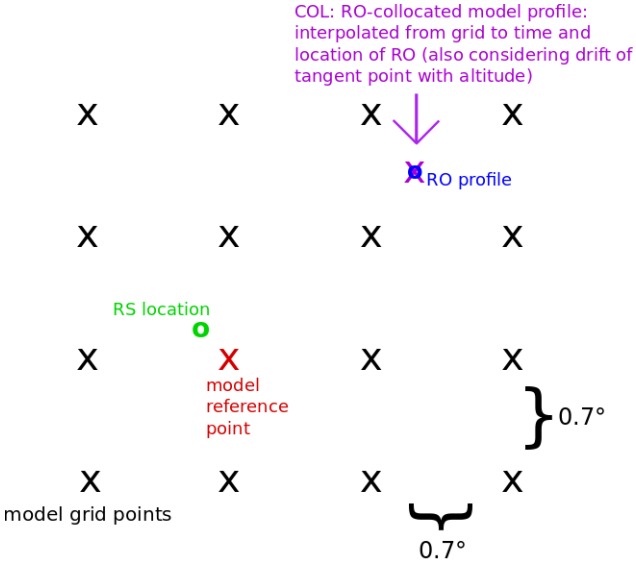

Figure 3. Schematic of the spatial correction applied to RO and RS co-location.

Office NWP background fields, in which the double-difference is applied to reduce the effects of temporal and spatial sampling errors. These studies use a double-difference sampling correction, but do not verify or discuss how the correction reduces sampling errors.

Here, we apply a spatial correction double-difference computed with model data and assess its effects on reducing sampling errors. We use ERA-Interim data to subtract the model background from both the RO and RS observations, removing spatial sampling differences and isolating the observational errors associated with the RO and RS pair. As shown in Fig. 3, we use the interpolated values of the ERA-Interim profiles at the RO location (eraPrf profiles provided by CDAAC) and use the ERA-Interim grid point nearest the RS location to compute the spatial correction. Due to the coarser vertical resolution of the ERA-Interim grid relative to the RS and RO vertical resolutions, comparisons with the spatial correction are conducted on a common 50 hPa uniform pressure grid from 1000 – 100 hPa to avoid further vertical interpolation.

The spatial corrected differences (X^{sc}) for the co-location pairs are computed as follows for the comparison variables (refractivity, temperature, and water vapor pressure):

$$X^{\mathrm{sc}} = (X_{\mathrm{RO}} - X_{\mathrm{ERA(RO)}}) - (X_{\mathrm{RS}} - X_{\mathrm{ERA(RS)}})$$
$$= (X_{\mathrm{RO}} - X_{\mathrm{RS}}) - (X_{\mathrm{ERA(RO)}} - X_{\mathrm{ERA(RS)}})$$

where $X_{\mathrm{ERA(RO)}}$ is the ERA-Interim model value interpolated to the RO location, $X_{\mathrm{ERA(RS)}}$ is the ERA-Interim model grid point value closet to the RS, and their difference, $X_{\mathrm{ERA(RO)}} - X_{\mathrm{ERA(RS)}}$, is referred to as the model correction term. We computed the RMS differences per pressure level on the 50 hPa grid.

Atmos. Meas. Tech. Discuss., https://doi.org/10.5194/amt-2018-20
Manuscript under review for journal Atmos. Meas. Tech.
Discussion started: 31 January 2018

Atmospheric Measurement Techniques Discussions

3 Results and discussion

Preliminary proof-of-concept testing of the ellipse method using only ERA-Interim data demonstrated a significant reduction in RMS refractivity differences within the ellipse relative to both the large circle and circles of similar area to the ellipse (not shown here). In the following two sections, aspects of the ellipse co-location are analyzed at the Lindenberg station. The final section presents the results of both the ellipse co-location and spatial correction at all four RS stations.

3.1 Filtered vs. unfiltered

Table 1. Unfiltered vs. filtered RMS percent differences* for refractivity, temperature, and water vapor pressure at Lindenberg, 2014. RMS differences are computed using all co-located pairs within 100 hPa pressure layers for the unfiltered and filtered data sets, then the percent differences between the two are computed and reported here.

Pressure (hPa)	Refractivity			Temperature			Water Vapor		
	large circle	small circle	ellipse	large circle	small circle	ellipse	large circle	small circle	ellipse
100 – 200	-2.94 %	-6.87 %	-5.96 %	-3.32 %	-7.99 %	-6.55 %	-0.68 %	-0.56 %	0.50 %
200 – 300	-1.28 %	-3.90 %	-2.34 %	-1.30 %	-4.12 %	-2.46 %	-0.78 %	-1.39 %	-1.65 %
300 – 400	-0.34 %	-0.90 %	-1.03 %	-0.20 %	-0.81 %	-0.71 %	-0.60 %	-0.53 %	-1.02 %
400 – 500	-0.80 %	-2.00 %	-1.22 %	-0.22 %	-0.76 %	-0.49 %	-1.03 %	-2.48 %	-1.32 %
500 – 600	-0.80 %	-1.87 %	-1.23 %	-0.30 %	-0.64 %	-0.49 %	-0.83 %	-2.17 %	-1.38 %
600 – 700	-1.05 %	-1.53 %	-1.36 %	-0.33 %	-0.65 %	-0.65 %	-1.03 %	-1.74 %	-1.59 %
700 – 800	-0.89 %	-1.51 %	-1.21 %	-0.26 %	-0.61 %	-0.65 %	-0.84 %	-1.54 %	-1.18 %
800 – 900	-0.97 %	-1.54 %	-1.12 %	-0.32 %	-0.57 %	-0.21 %	-0.85 %	-1.44 %	-0.99 %
900 – 1000	-0.62 %	-0.65 %	-0.94 %	-0.37 %	-0.41 %	-0.26 %	-0.48 %	-0.61 %	-0.79 %

*percent differences computed as 100 * (RMS_{filt} – RMS_{unfilt}) / RMS_{unfilt}

Filtering both the RO and RS profiles has a small, positive impact on reducing RMS differences in refractivity, temperature, and water vapor pressure. Compared to RMS differences computed using the unfiltered profiles at Lindenberg, filtering both the RO and RS profiles before co-location reduces RMS differences by about 1 % on average, up to almost 8 % in some instances (see Table 1). Based on these results, to reduce representativeness errors we filtered all RO and RS profiles before computing their differences.

3.2 Effects of wind speed on ellipse co-location

The relationship between the wind direction and horizontal variability (and sampling error) of refractivity is expected to break down for light wind speeds, and indeed we found that if wind speeds are low, the effectiveness of orienting the ellipse along the direction of wind flow is significantly reduced. We separated co-located RO–RS pairs at Lindenberg into two groups based on the reported wind speed of the RS at a given time and pressure level: (1) wind speeds less than 5 $\mathrm{m\,s^{-1}}$ and (2) wind speeds greater than or equal to 5 $\mathrm{m\,s^{-1}}$. Figure 4 shows the RMS differences in refractivity for each group.

Atmos. Meas. Tech. Discuss., https://doi.org/10.5194/amt-2018-20
Manuscript under review for journal Atmos. Meas. Tech.
Discussion started: 31 January 2018

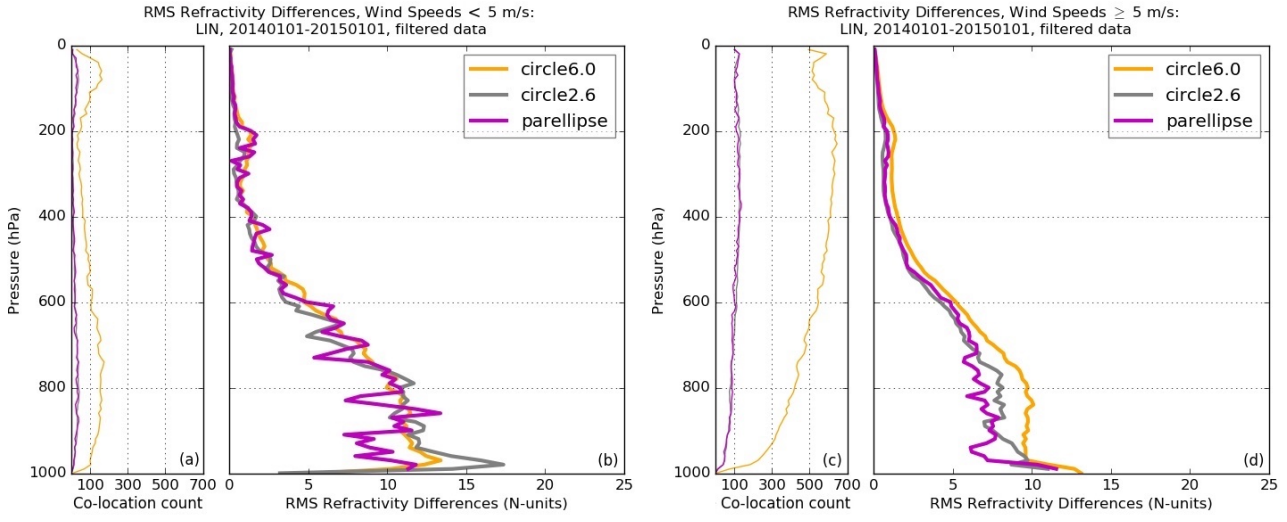

Figure 4. RMS refractivity differences at Lindenberg 2014 for two sets of RO–RS pairs separated by reported RS wind speeds: pairs with wind speeds less than $5\,\mathrm{m\,s^{-1}}$ (left) and pairs with RS wind speeds greater than or equal to $5\,\mathrm{m\,s^{-1}}$ (right). Geometric constraints are shown in the following colors: large circle (orange), small circle (grey), and ellipse (magenta).

As shown in Fig. 4, the clear distinction between RMS profiles for the ellipse and two circles when wind speeds are greater than $5\,\mathrm{m\,s^{-1}}$ essentially vanishes when wind speeds are less than $5\,\mathrm{m\,s^{-1}}$. Similarities in RMS refractivity differences when wind speeds are less than $5\,\mathrm{m\,s^{-1}}$ are likely associated with greater atmospheric homogeneity and weaker gradients in the region, resulting in similar observations within the area containing both circles and the ellipse. When wind speeds increase to larger than $5\,\mathrm{m\,s^{-1}}$, there is a greater separation between the circles and ellipse with respect to the RMS difference. Under moderate to high wind speed conditions, the ellipse reduces RMS refractivity differences relative to both the large and small circle, particularly below about 700 hPa. In the upper troposphere, both the ellipse and the smaller circle give similar results and smaller RMS differences than the large circle (Fig. 4). In the case of Lindenberg, since the majority of wind speeds are greater than $5\,\mathrm{m\,s^{-1}}$ (as noted by the differences in co-location counts under the two wind constraints in Fig. 4), low wind speeds do not have a significant effect on the overall RMS differences when co-location pairs are not separated by wind speed (see Fig. 5).

3.3 Ellipse co-location and spatial correction applied at four RS stations

We carried out two RO–RS comparisons at four different RS locations (Lindenberg, Ny-Ålesund, Tateno, and Nauru): first we compared pairs with RO observations co-located within the large circle, small circle, and ellipse centered at the RS station, and second, we applied the spatial correction to the RO–RS pairs within the ellipse and two circles. We then computed RMS differences in refractivity, temperature, and water vapor pressure.

Atmos. Meas. Tech. Discuss., https://doi.org/10.5194/amt-2018-20
Manuscript under review for journal Atmos. Meas. Tech.
Discussion started: 31 January 2018

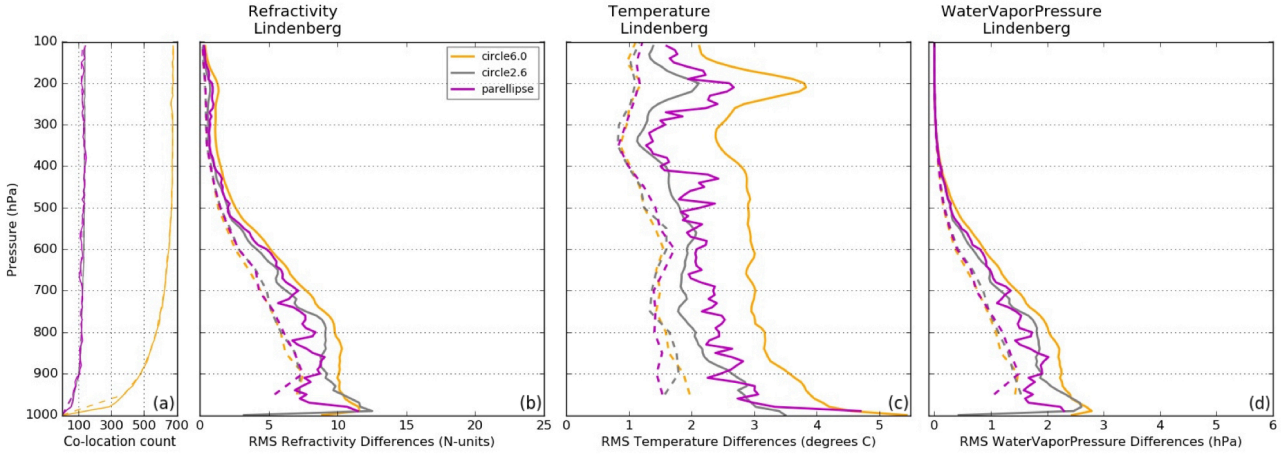

Figure 5. RMS differences for RO–RS co-locations at Lindenberg, 2014. RMS differences with ellipse method only (solid; large circle: orange, small circle: grey, ellipse: magenta) and RMS differences with ellipse method and spatial correction (dashed) are shown for all three variables: (b): refractivity, (c): temperature, (d): water vapor pressure. The number of pairs within each ellipse (solid) and ellipse plus spatial correction (dashed) are shown in (a).

Figure 5 illustrates the RMS differences for refractivity, temperature, and water vapor pressure with and without the spatial correction at Lindenberg. Considering the ellipse method only (solid lines), the ellipse reduces RMS differences relative to the large circle for all three variables at all pressure levels, having the most significant reduction in the temperature RMS differences. Generally, the small circle and ellipse have similar RMS differences, however there are pressure layers in which the ellipse reduces the RMS relative to the small circle. When the spatial correction is applied to the circles and ellipse (dashed lines), the RMS differences are significantly reduced and converge with minimal differences between the ellipse and circles.

The RMS differences at Lindenberg are mostly affected by spatial sampling errors; temporal sampling errors are minimized by the reduced time window of 1 h due to frequent (four times daily) RS launches at this station. The ellipse decreases RMS differences relative to both circles, effectively reducing spatial sampling errors driven by atmospheric variability. The spatial correction is most effective at reducing spatial sampling errors, particularly for the large circle in which atmospheric variability is more likely.

The results at Ny-Ålesund and Tateno are very similar to those at Lindenberg, with some minor differences in the lower troposphere (Fig. 6). Again, using pairs in the ellipse only (solid, magenta) reduces RMS differences relative to the large circle (solid, orange) and is equal to or less than RMS differences within the small circle (solid, grey). Including the spatial correction shows the largest reduction in RMS differences such that the differences from all three geometric types converge to similar values. At both Ny-Ålesund and Tateno, the reduction of RMS differences in the ellipse compared to the large circle becomes less in the lower troposphere (below 800 hPa) where the frequency of wind speeds less than $5\,\mathrm{m\,s^{-1}}$ increase and the relationship between wind direction and RO–RS differences breaks down. For example, at Ny-Ålesund and Tateno the

Atmos. Meas. Tech. Discuss., https://doi.org/10.5194/amt-2018-20
Manuscript under review for journal Atmos. Meas. Tech.
Discussion started: 31 January 2018

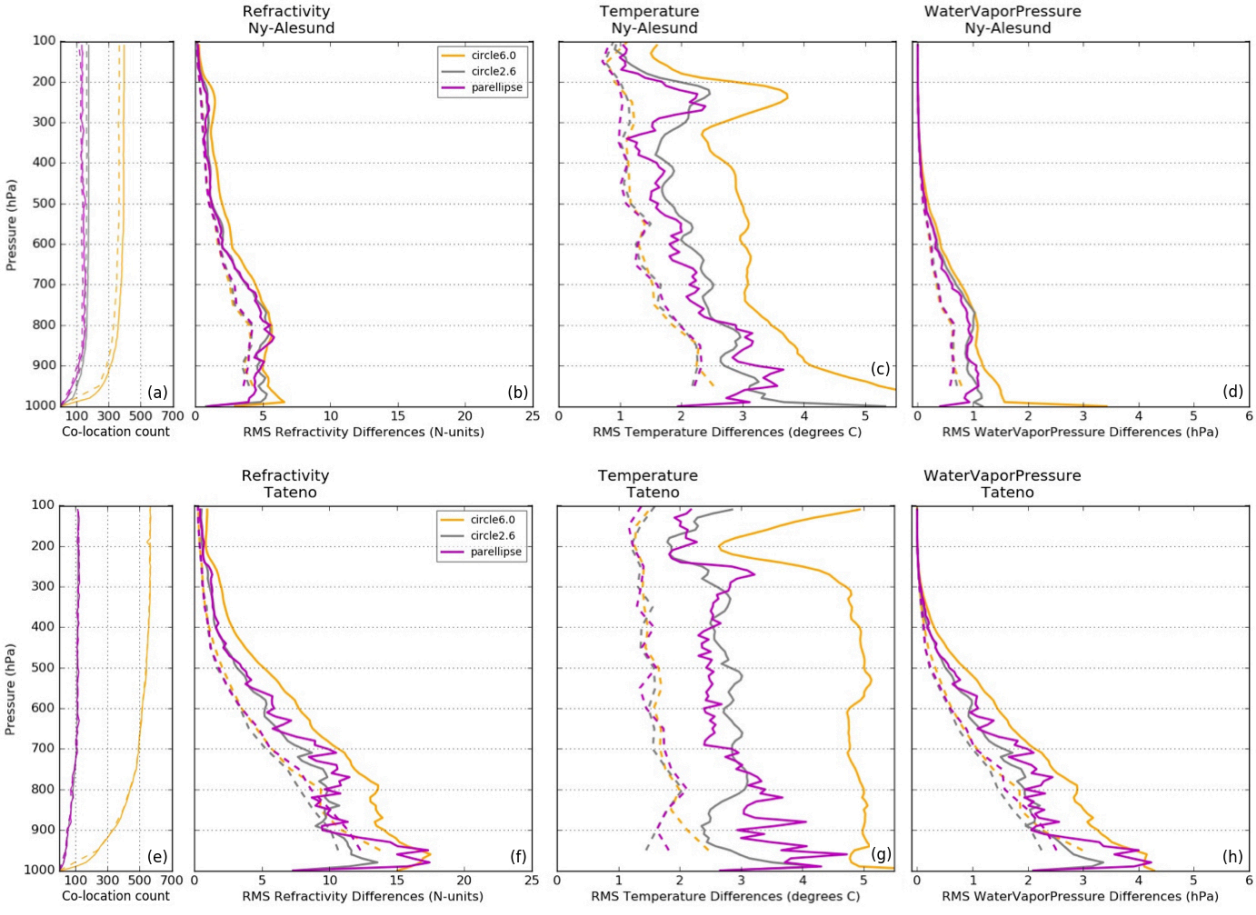

Figure 6. Same as Fig. 5 for two different locations: Ny-Ålesund, 2013 (a-d) and Tateno, 2012 (e-h).

percentages of RO–RS pairs for which the wind speed is less than $5\,\mathrm{m\,s^{-1}}$ are 36.1 % and 32.7 % respectively. The small sample size in the ellipse compared to the large circle (Fig. 6) may also play a role, allowing a few outliers to dominate the statistics.

The tropical location of Nauru generally confirms the findings at the other three RS locations. The ellipse alone (Fig. 7, solid, magenta) decreases RMS differences relative to the large circle (solid, orange) and is comparable to the RMS differences of the small circle (solid, grey). There is less distinction, however, between the ellipse method only (solid) and spatial correction (dashed) RMS differences, particularly for temperature. All six geometric and spatial correction combinations have overlapping RMS temperature differences and show little separation between co-location methods, unlike the results at Lindenberg, Ny-Ålesund, and Tateno. This is most likely caused by the relative horizontal homogeneity in temperature at Nauru, which is located in the deep tropics. Thus, there is little to no distinction between RMS temperature differences using various geometrical constraints or spatial correction.

Atmos. Meas. Tech. Discuss., https://doi.org/10.5194/amt-2018-20
Manuscript under review for journal Atmos. Meas. Tech.
Discussion started: 31 January 2018

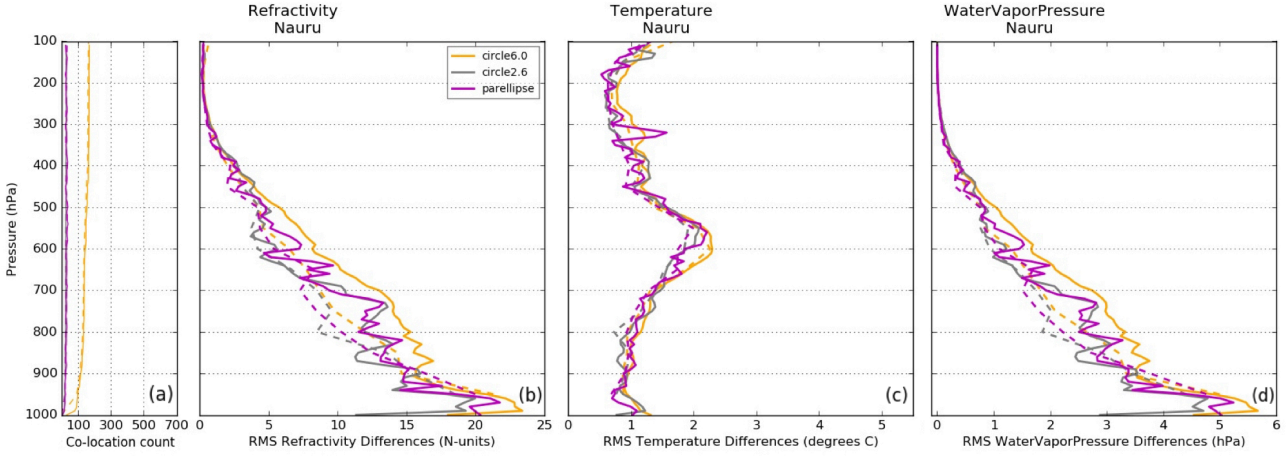

Figure 7. Same as Fig. 5 for Nauru, 2011-2013.

Refractivity and water vapor pressure RMS differences in the lower troposphere ($1000 - 700\,\mathrm{hPa}$) at Nauru are the largest of the four stations, caused primarily by atmospheric conditions at its location in the deep tropics. RO is known to have negative refractivity biases in the lower troposphere, particularly in moist tropical regions where large water vapor and associated refractivity gradients often result in super-refraction (Rocken et al., 1997; Ao et al., 2003; Sokolovskiy, 2003; Beyerle et al., 2006; Anthes et al., 2008). Overall, this results in larger RMS refractivity differences at Nauru. Since super-refraction is an error characteristic of RO retrievals and not related to horizontal sampling errors, the spatial correction has no impact on the RO–RS refractivity differences.

4 Conclusions

We have shown that vertical filtering of the RO and RS profiles before comparison reduces representativeness errors associated with different vertical resolutions and observation types by a small amount (typically a few percent). Using these filtered profiles, we tested two methods to reduce sampling errors during RO–RS co-location comparisons: (1) restricting RO and RS pairs to within ellipses oriented along the direction of wind flow and (2) applying a spatial correction using model data to remove differences caused by horizontal atmospheric gradients. When wind speeds exceed about $5\,\mathrm{m\,s^{-1}}$, co-locations within the ellipse parallel to the wind flow reduce RMS differences in refractivity, temperature, and water vapor pressure relative to co-locations within the large circle, and either reduce or are equal to RMS differences within the smaller circle. The effectiveness of co-locating RO–RS pairs within the ellipse is reduced for wind speeds less than $5\,\mathrm{m\,s^{-1}}$.

Applying the spatial correction using ERA-Interim model data showed the most significant reduction in RMS differences, more-so than applying the ellipse constraint alone. The spatial correction reduced RMS differences in refractivity, temperature, and water vapor pressure by an average of 55 %. The reductions of sampling errors within both large and small circles and

the ellipse tend to converge with the spatial correction applied, rendering the differences in geometric constraints of the circles and ellipse negligible. An exception to this reduction in RMS occurs at Nauru in the lower troposphere, where super-refraction associated with the atmospheric conditions of the deep tropics tends to dominate the RMS differences.

In order to reduce sampling errors for future RO–RS co-location comparisons, our results suggest that applying the spatial correction under more lenient co-location criteria would be most effective. By using a large distance constraint, the sample size will be sufficiently large and applying the spatial correction eliminates most sampling errors, even for the large distance restriction (greater than 600 km). However, if a reliable model is unavailable, restricting co-locations within ellipses oriented along the direction of wind flow will help to reduce sampling errors caused by atmospheric variability. Both of these methods are effective in reducing sampling errors caused by spatial and temporal differences during comparisons and should provide a more accurate error analysis of RO and RS observations.

Code availability. The code used in this study will be made available upon request.

Data availability. The data used in this study will be made available upon request.

Author contributions. TR and RA developed the idea and contributed through the entirety of this project. SG conducted the majority of the coding, data retrieval, and computations and analysis, with TR contributing to coding and data retrieval. SG prepared the manuscript with contributions from both co-authors.

Competing interests. The authors declare that they have no conflict of interest.

Acknowledgements. The authors thank Drs. Eric DeWeaver (NSF) and Jack Kaye (NASA) for their support of this research through NSF-NASA grant AGS-1522830. Dr. Sergey Sokolovskiy provided many useful comments and suggestions during this study. The first author was supported in part by the Significant Opportunities in Atmospheric Research and Science (SOARS) program, NSF grant AGS-1641177, and by the Constellation Observing System for Meteorology, Ionosphere, and Climate (COSMIC) program at UCAR, which is sponsored by the National Space Office in Taiwan, NSF, NASA, NOAA, and the U.S. Air Force. Thanks to CDAAC for the provided RO data sets and NOAA NCDC and GRUAN for the provided RS data sets. The first and second author would like to thank Dr. Keith Maull for his suggestions during this study.

References

Anthes, R., Bernhardt, P., Chen, Y., Cucurull, L., Dymond, K., Ector, D., Healy, S., Ho, S.-P., Hunt, D., Kuo, Y.-H., Liu, H., Manning, K., McCormick, C., Meehan, T., Randel, W., Rocken, C., Schreiner, W., Sokolovskiy, S., Syndergaard, S., Thompson, D. C., Trenberth, K., Wee, T.-K., Yen, N., and Zeng, Z.: The COSMIC/FORMOSAT-3 Mission-Early Results, Bull. Amer. Meteor. Soc., 89, 313–333, https://doi.org/10.1175/BAMS-89-3-31, 2008.

Anthes, R. A.: Exploring Earth's atmosphere with radio occultation: contributions to weather, climate, and space weather, Atmos. Meas. Tech., 4, 1077–1103, https://doi.org/10.5194/amt-4-1077-2011, 2011.

Ao, C., Meehan, T., Hajj, G., Mannucci, A., and Beyerle, G.: Lower troposphere refractivity bias in GPS occultation retrievals, J. Geophys. Res., 108, https://doi.org/10.1029/2002JD003216, 2003.

Beyerle, G., Schmidt, T., Wickert, J., Heise, S., Rothacher, M., Konig-Langlo, G., and Lauristen, K.: Observations and simulations of receiver-induced refractivity biases in GPS radio occultation, J. Geophys. Res., 111, https://doi.org/10.1029/2005JD006673, 2006.

Dirksen, R., Sommer, M., Immler, F., Hurst, D., Kivi, R., and Vömel, H.: Reference quality upper-air measurements: GRUAN data processing for the Vaisala RS92 radiosonde, Atmos. Meas. Tech., 7, 4463–4490, https://doi.org/10.5194/amt-7-4463-2014, 2014.

Haimberger, L., Tavolato, C., and Sperka, S.: Homogenization of the global radiosonde temperature dataset through combined comparison with reanalysis background series and neighboring stations, J. Climate, 25, 8108–8131, https://doi.org/10.1175/JCLI-D-11-00668.1, 2012.

He, W., Ho, S.-P., Chen, H., Zhou, X., Hunt, D., and Kuo, Y.-H.: Assessment of radiosonde temperature measurements in the upper troposphere and lower stratosphere using COSMIC radio occultation data, Geophys. Res. Lett., 36, https://doi.org/10.1029/2009GL038712, 2009.

Ho, S.-P., Zhou, X., Kuo, Y.-H., Hunt, D., and Wang, J.: Global evaluation of radiosonde water vapor systematic biases using GPS radio occultation from COSMIC and ECMWF analysis, Remote Sensing, 2, 1320–1330, https://doi.org/10.3390/rs2051320, 2010.

Ho, S.-P., Peng, L., and Vömel, H.: Characterization of the long-term radiosonde temperature bias in the upper troposphere and lower stratosphere using COSMIC and Metop-A/GRAS data from 2006 to 2014, Atmos. Chem. Phys., 17, 4493–4511, https://doi.org/10.5194/acp-17-449-2017, 2017.

Kuo, Y.-H., Wee, T., Sokolovskiy, S., Rocken, C., Schreiner, W., Hunt, D., and Anthes, R.: Inversion and error estimation of GPS radio occultation data, J. Meteor. Soc. Japan, 82, 507–531, https://doi.org/10.2151/jmsj.2004.507, 2004.

Kuo, Y.-H., Schreiner, W., Wang, J., Rossiter, D., and Zhang, Y.: Comparison of GPS radio occultation soundings with radiosondes, Geophys. Res. Lett., 32, https://doi.org/10.1029/2004GL021443, 2005.

Kursinski, E., Hajj, G., Schofield, J., Linfield, R., and Hardy, K.: Observing Earth's atmosphere with radio occultation measurements using the Global Positioning System, J. Geophys. Res., 102, 23 429–23 465, https://doi.org/10.1029/97JD01569, 1997.

Ladstädter, F., Steiner, A., Schwärz, M., and Kirchengast, G.: Climate intercomparison of GPS radio occultation, RS90/92 radiosondes and GRUAN from 2002 to 2013, Atmos. Meas. Tech., 8, 1819–1834, https://doi.org/10.5194/amt-8-1819-2015, 2015.

Melbourne, W., Davis, E., Duncan, C., Hajj, G., Hardy, K., Kursinski, E., Meehan, T., Young, L., and Yunck, T.: The application of space borne GPS to atmospheric limb sounding and global change monitoring, Tech. rep., Jet Propulsion Lab., California Institute of Technology, 1994.

Rocken, C., Anthes, R. A., Exner, M., Hunt, D., Sokolovskiy, S., Ware, R., Gorbunov, M., Schreiner, W., Feng, D., Herman, B., Kuo, Y.-H., and Zou, X.: Analysis and validation of GPS/MET data in the neutral atmosphere, J. Geophys. Res., 102, 29 849–29 866, https://doi.org/10.1029/97JD02400, 1997.

Savitzky, A. and Golay, M.: Analytical Chemistry, 36, 1627–1639, 1964.

Smith, E. K. and Weintraub, S.: The constants in the equation for atmospheric refractive index at radio frequencies, Proceedings of the IRE, 41, 1035–1037, 1953.

Sokolovskiy, S.: Effect of superrefraction on inversions of radio occultation signals in the lower troposphere, Radio Sci., 38, https://doi.org/10.1029/2002RS002728, 2003.

Staten, P. and Reichler, T.: Apparent precision of GPS radio occultation temperatures, Geophys. Res. Lett., 36, https://doi.org/10.1029/2009GL041046, 2009.

Sun, B., Reale, A., Seidel, D. J., and Hunt, D. C.: Comparing radiosonde and COSMIC atmospheric profile data to quantify differences among radiosonde types and the effects of imperfect collocation on comparison statistics, J. Geophys. Res., 115, https://doi.org/10.1029/2010JD014457, 2010.

Tradowsky, J., Burrows, C., Healy, S., and Eyre, J.: A new method to correct radiosonde temperature biases using radio occultation data, J. Appl. Meteor. Climatol., 56, 1643–1661, https://doi.org/10.1175/JAMC-D-16-0136.1, 2017.

Vergados, P., Mannucci, A., and Ao, C.: Assessing the performance of GPS radio occultation measurements in retrieving tropospheric humidity in cloudiness: A comparison study with radiosondes, ERA-Interim, and AIRS data sets, J. Geophys. Res., 19, 7718–7731, https://doi.org/10.1002/2013JD021398, 2014.

Wang, B.-R., Liu, X., and Wang, J.-K.: Assessment of COSMIC radio occultation retrieval products using global radiosonde data, Atmos. Meas. Tech., 6, 1073–2013, https://doi.org/10.5194/amt-6-1073-2013, 2013.

Ware, R., Exner, M., Feng, D., Gorbunov, M., Hardy, K., Herman, B., Kuo, Y.-H., Meehan, T., Melbourne, W., Rocken, C., Schreiner, W., Sokolovskiy, S., Solheim, F., Zou, X., Anthes, R. A., Businger, S., and Trenberth, K.: GPS sounding of the atmosphere from low earth orbit: Preliminary results, Bull. Amer. Meteor. Soc., 77, 19–40, https://doi.org/10.1175/1520-0477(1996)077<0019:GSOTAF>2.0.CO;2, 1996.

Wickert, J., Schmidt, T., Beyerle, G., Konig, R., and Reigber, C.: The radio occultation experiment aboard CHAMP: Operational data analysis and validation of vertical atmospheric profiles, J. Meteor. Soc. Japan, 82, 381–395, https://doi.org/10.2151/jmsj.2004.381, 2004.

Wong, S., Fetzer, E., Schreier, M., Manipon, G., Fishbein, E., Kahn, B., Yue, Q., and Irion, F.: Cloud-induced uncertainties in AIRS and ECMWF temperature and specific humidity, J. Geophys. Res., 120, 1880–1901, https://doi.org/10.1002/2014JD022440, 2015.

Xu, X., Luo, J., and Shi, C.: Comparison of COSMIC radio occultation refractivity profiles with radiosonde measurements, Adv. Atmos. Sci., 26, 1137–1145, https://doi.org/10.1007/s00376-009-8066-y, 2009.

Zhang, K., Fu, E., Silcock, D., Wang, Y., and Kuleshov, Y.: An investigation of atmospheric temperature profiles in the Australian region using collocated GPS radio occultation and radiosonde data, Atmos. Meas. Tech., 4, 2087–2092, https://doi.org/10.5194/amt-4-2087-2011, 2011.